ILLiad Request Printout

Transaction Number: 182676
Username: StuartHudson Name: Stuart Hudson Status: F - Faculty
ISSN/ISBN: ISSN: 0022-3778
NotWantedAfter: 08/03/2005
Accept Non English: No
Accept Alternate Edition: No
Request Type: Article - ArticleExpress

Loan Information

LoanAuthor:
LoanTitle:
LoanPublisher:
LoanPlace:
LoanDate:
LoanEdition:
NotWantedAfter: 08/03/2005

Article Information

PhotoJournalTitle: Journal of Plasma Physics
PhotoJournalVolume: 56
PhotoJournalIssue: 2
Month: Oct
Year:
Pages: 361
Article Author: Hudson, Dewar
Article Title: Almost-invariant surfaces for magnetic field-line flows

Citation Information

Cited In:
Cited Title:
Cited Date:
Cited Volume:
Cited Pages:

OCLC Information

ILL Number:
OCLC Number:
Lending String:
Original Loan Author:
Original Loan Title:
Old Journal Title:
Call Number: QC718 .J6
Location: Harold P. Furth Plasma Physics Library (PPL)

Notes

2/4/2005 1:54:40 PM jes Accession number: 96123476920

J. Plasma Physics (1996), *vol.* 56, *part* 2, *pp.* 361–382

Almost-invariant surfaces for magnetic field-line flows

By S.R. HUDSON AND R.L. DEWAR

Department of Theoretical Physics and Plasma Research Laboratory,
Research School of Physical Sciences and Engineering,
The Australian National University,
Canberra ACT 0200, Australia†

(Received 27 October 1995)

Two approaches to defining almost-invariant surfaces for magnetic fields with imperfect magnetic surfaces are compared. Both methods are based on treating magnetic field-line flow as a $1\frac{1}{2}$-dimensional Hamiltonian (or Lagrangian) dynamical system. In the *quadratic-flux minimizing surface* approach, the integral of the square of the action gradient over the toroidal and poloidal angles is minimized, while in the *ghost surface* approach a gradient flow between a minimax and an action-minimizing orbit is used. In both cases the almost-invariant surface is constructed as a family of periodic pseudo-orbits, and consequently it has a rational rotational transform. The construction of quadratic-flux minimizing surfaces is simple, and easily implemented using a new magnetic field-line tracing method. The construction of ghost surfaces requires the representation of a pseudo field line as an (in principle) infinite-dimensional vector and also is inherently slow for systems near integrability. As a test problem the magnetic field-line Hamiltonian is constructed analytically for a topologically toroidal, non-integrable *ABC*-flow model, and both types of almost-invariant surface are constructed numerically.

1. Introduction

In the classical dynamics of Hamiltonian systems (Goldstein 1980), one typically seeks to transform to coordinates such that the vector field describing the differential equations of motion leaves a set of phase-space coordinates, the new momenta, constant. These constant momenta are called the *actions*, and when they exist the system is called *integrable*. If the phase-space motions are bounded, the constant-action surfaces must be tori, and the variables canonically conjugate to the actions are called the *angles*.

In this paper we restrict attention to the so-called $1\frac{1}{2}$-degree of freedom systems, where there is only one momentum and one angle-like configuration-space coordinate, but the system is periodically forced in time, so that the phase of the external perturbation can be regarded as a second angle variable. The extended phase space is thus three-dimensional. Such a system is said to be integrable if all trajectories in the extended phase space lie on invariant two-tori, which form a one-parameter family filling (foliating) the extended phase space.

† e-mail: stuart.hudson@anu.edu.au, robert.dewar@anu.edu.au.

A similar problem occurs in toroidal plasma confinement, where for improved confinement one seeks a magnetic vector field such that the field lines remain on toroidal surfaces. By considering such flux surfaces, when they exist, as coordinate surfaces, one may define preferred curvilinear coordinate systems, such as Boozer coordinates (Boozer 1982) in analogy with action-angle coordinates. In fact (see § 2.1) the two problems are identical, since field-line flow in systems such as stellarators, which lack a continuous symmetry, forms a $1\frac{1}{2}$-degree-of-freedom Hamiltonian system. The field-line problem is thus an important application of the general theory of such systems and one where the extended phase space has a clear physical meaning, being the real three-dimensional configuration space in which magnetic fields exist.

Since $1\frac{1}{2}$-degree-of-freedom Hamiltonian systems are not generically integrable, the existence of nested flux surfaces in magnetic confinement devices is the exception rather than the rule, with field lines following chaotic trajectories that are not confined to a two-torus. With careful design, the regions of chaos can be reduced (Hanson & Cary 1984; Cary & Hanson 1986; Hanson 1994) and the magnetic field becomes nearly integrable. To investigate deviations of the field from integrability, one may compare the true motion against motion in an integrable system that is as close as possible to the actual system (Boozer 1983; Kaasalainen & Binney 1994). We call the action-angle variables and invariant surfaces of such a neighbouring integrable system *approximate* action-angle variables and *almost*-invariant surfaces for the true system.

The concept of 'as close as possible' is clearly not uniquely defined. In this paper we seek to compare two approaches to this problem, based on the construction of selected almost-invariant tori rather than of a full set of approximate action-angle variables. This approach has the advantage that the construction of each surface may be done independently, thus reducing the dimensionality of the problem by one.

At first sight, it might appear natural to select the candidate almost-invariant tori to have irrational rotation numbers (rotational transforms) since, by the Kolmogorov–Arnol'd–Moser (KAM) theorem (Arrowsmith & Place 1991; Lichtenberg & Lieberman 1992), such tori can survive as truly invariant tori even after an integrable system is perturbed into a non-integrable one. One would require the algorithm for defining 'almost-invariant' to be such that it found a KAM surface when it exists. However, KAM surfaces are fragile, and their disappearance is difficult to predict precisely (Greene 1979). After breakup of a KAM torus, the remaining invariant set has a Cantor-set structure.

The rational rotation numbers, on the other hand, have simple invariant sets associated with them – the closed, periodic orbits corresponding to the X- and O-points of island chains – which survive to arbitrarily large perturbation (Arrowsmith & Place 1991; Lichtenberg & Lieberman 1992), and can be readily incorporated into robust almost-invariant tori. The problem then becomes to 'fill in the gaps' between the periodic orbits. In both algorithms used in this paper this is accomplished by defining a one-parameter family of periodic 'pseudo-orbits' that include the true periodic orbits of an island chain. Because KAM surfaces, when they exist, can be approximated arbitrarily closely by periodic orbits of sufficiently high-order rational rotation numbers (Greene 1979), no generality is in fact lost by restricting attention to rational rotation numbers.

Both of the approaches that we shall use are connected with Hamilton's princi-

ple in that they can be viewed as seeking to minimize the gradient of the action in different ways. Ghost curves (Angenent & Golé 1991; Golé 1992; MacKay & Muldoon 1993; Dewar & Khorev 1995) for area-preserving twist maps are defined as a flow under the gradient of the action defined on the finite-dimensional space of coordinates of a periodic pseudo-orbit. We generalize this to continuous-time Hamiltonian systems by using the variational derivative of the Lagrangian as the action gradient. Ghost surfaces are then defined using the gradient flow of the action on the space of periodic curves in phase space. We implement this numerically by using piecewise-linear pseudo-orbits in Hamilton's principle to discretize the problem.

The other candidates for almost-invariant tori are the quadratic-flux minimizing surfaces of Dewar *et al.* (1994). Such a surface is defined, for divergence-free fields, as a stationary point of the integral over any toroidal trial surface of the square of the normal component of the field, with a weighting function chosen to make the Euler–Lagrange equation have non-singular solutions. We show in this paper that quadratic-flux minimizing surfaces can be defined, for general Hamiltonian systems, as the integral of the square of the action gradient. The weight function is then seen to arise naturally. These surfaces are closely related to the quadratic-flux minimizing curves recently introduced for area-preserving twist mappings (Dewar & Meiss 1992; Dewar & Khorev 1995).

In § 2 we review the Lagrangian and Hamiltonian formulations of magnetic field-line flow. In § 3 ghost-surfaces are defined and an expression for the action along a piecewise linear trial curve is given. Expressions for the action gradient and Hessian are given in the appendix. In § 4 quadratic-flux minimizing surfaces are defined, and the concept of pseudo-orbits is used to interpret the Euler-Lagrange equation. For illustration, in § 5 we introduce a simple non-integrable, topologically toroidal system, formed by superimposing a periodic ABC flow with a linearly sheared slab field. In the last sections, quadratic-flux minimizing surfaces and ghost surfaces are displayed and compared.

2. Magnetic fields as dynamical systems

2.1. *Field-line Hamiltonian*

Toroidal magnetic vector fields are equivalent to time-dependent $1\frac{1}{2}$-degree-of-freedom Hamiltonian systems (Boozer 1983; Cary & Littlejohn 1983; D'haeseleer *et al.* 1983; Lichtenberg & Lieberman 1992; Yoshida 1994). To see this, we start from the result (Boozer 1983; Yoshida 1994) that a general non-integrable magnetic field in a toroidal system can be represented in the form

$$\mathbf{B}(\mathbf{r}) = \nabla\psi \times \nabla\theta + \nabla\zeta \times \nabla\chi\,, \tag{2.1}$$

where $\theta(\mathbf{r})$ and $\zeta(\mathbf{r})$ are respectively generalized poloidal and toroidal angle coordinate functions, and $\psi(\mathbf{r})$ and $\chi(\mathbf{r})$ are respectively toroidal and poloidal flux functions whose level surfaces do not in general coincide. We now introduce a third generalized coordinate $\rho(\mathbf{r})$ whose level surfaces form tori nested about the singular line of the θ coordinate, so that (ρ, θ, ζ) forms a complete curvilinear coordinate system, and write $\chi = \bar{\chi}(\rho, \theta, \zeta)$ and $\psi = \bar{\psi}(\rho, \theta, \zeta)$. The flux functions can now be constructed from the contravariant components $B^\theta \equiv \mathbf{B}.\nabla\theta$, $B^\zeta \equiv \mathbf{B}.\nabla\zeta$ and

$B^\rho \equiv \mathbf{B}.\nabla\rho$ by integrating the differential equations

$$\partial_\rho \bar{\chi}(\rho,\theta,\zeta) = \bar{\mathcal{J}} B^\theta \,, \tag{2.2}$$

$$\partial_\rho \bar{\psi}(\rho,\theta,\zeta) = \bar{\mathcal{J}} B^\zeta \,, \tag{2.3}$$

$$\partial_\zeta \bar{\psi} + \partial_\theta \bar{\chi} = -\bar{\mathcal{J}} B^\rho \,, \tag{2.4}$$

where the overbar denotes a field expressed as a function of ρ, θ and ζ (since we wish below to use the unbarred symbol to imply dependence on ψ, θ and ζ) and $\bar{\mathcal{J}} \equiv (\nabla\rho.\nabla\theta \times \zeta)^{-1}$ is the Jacobian in (ρ,θ,ζ) coordinates. Equations (2.2)–(2.4) must usually be solved numerically, but in this paper we use a model where they can be evaluated analytically (see § 5).

Assuming $\partial_\rho \bar{\psi} \neq 0$, we can invert $\psi = \bar{\psi}(\rho,\theta,\zeta)$ to obtain

$$\rho = \rho(\psi,\theta,\zeta) \,, \tag{2.5}$$

so we replace ρ by ψ as the independent generalized radial coordinate and express the poloidal flux function as

$$\chi = \chi(\psi,\theta,\zeta) \,. \tag{2.6}$$

Assuming $B^\zeta \neq 0$ at any point, the value of ζ can be used to parametrize the position along a field line, and the evolution of a point on the line as ζ increases can be described by the differential equations

$$\frac{d\theta}{d\zeta} = \frac{\mathbf{B}.\nabla\theta}{\mathbf{B}.\nabla\zeta} \,, \quad \frac{d\psi}{d\zeta} = \frac{\mathbf{B}.\nabla\psi}{\mathbf{B}.\nabla\zeta} \,. \tag{2.7}$$

Using (2.1) and (2.6), we write these equations of motion in the form

$$\dot{\theta} = \frac{\partial\chi}{\partial\psi} \,, \tag{2.8}$$

$$\dot{\psi} = -\frac{\partial\chi}{\partial\theta} \,. \tag{2.9}$$

where the dot represents the derivative with respect to ζ. These equations are recognized as Hamilton's equations, with ζ acting like a time coordinate, ψ playing the role of the momentum conjugate to the angular position coordinate θ, and χ being the Hamiltonian. By using ψ as the radial variable, we have obtained the equations in canonical form, but it would be possible to work with a general radial coordinate ρ at the expense of a non-canonical form of Hamilton's equations (Cary & Littlejohn 1983).

2.2. *Field-line Lagrangian and action*

Assume $\partial^2\chi/\partial\psi^2 \neq 0$, so that (2.8) is invertible to give the momentum in terms of the velocity, $\psi = \psi(\theta,\dot{\theta},\zeta)$ The field-line Lagrangian $\varphi = \varphi(\theta,\dot{\theta},\zeta)$ is constructed from the Hamiltonian in the usual way (Goldstein 1980):

$$\varphi = \psi\dot{\theta} - \chi \,. \tag{2.10}$$

The action S is defined for some specified curve $\gamma = \theta(\zeta)$, as the 'time' integral of the Lagrangian:

$$S[\gamma] = \int_\gamma \varphi \, d\zeta \quad \text{along the curve } \gamma : \ \theta = \theta(\zeta) \,. \tag{2.11}$$

From Hamilton's principle (Goldstein 1980), S is stationary with respect to variations of γ when γ is an actual field line. Note that (2.8) is automatically satisfied

during variation of S, by construction, but that the second of the Hamiltonian equations of motion, (2.9), has not been used, and will be violated except at stationary points of S.

Regarding $\theta(\zeta)$ as a vector in an infinite-dimensional function space, and S as a scalar function of that vector, Hamilton's principle is the statement that the gradient of S vanishes on a physical field line. To see this, we vary the curve γ along which the Lagrangian is integrated,

$$\theta(\zeta) \rightarrow \theta(\zeta) + \delta\theta(\zeta) \,, \tag{2.12}$$

and define the variational or Fréchet derivative $\delta S/\delta\theta$ such that

$$\delta S \equiv \int_\gamma \frac{\delta S}{\delta\theta}\delta\theta \, d\zeta \qquad \forall\delta\theta \,. \tag{2.13}$$

(There are no endpoint contributions because of the assumed periodicity of the system.) Since δS is the inner product of $\delta\theta$ and $\delta S/\delta\theta$ for all $\delta\theta$, $\delta S/\delta\theta$ is the natural generalization of the gradient. From the action integral (2.11), using integration by parts,

$$\frac{\delta S}{\delta\theta} = \frac{\partial\varphi}{\partial\theta} - \frac{d}{d\zeta}\frac{\partial\varphi}{\partial\dot{\theta}} \,. \tag{2.14}$$

The usual Euler–Lagrange equations are obtained when the gradient $\delta S/\delta\theta$ is set equal to zero, as was to be proved.

Substituting (2.10) into (2.14), we find the Hamiltonian form of the action gradient,

$$\frac{\delta S}{\delta\theta} = -\left(\dot{\psi} + \frac{\partial\chi}{\partial\theta}\right) \,, \tag{2.15}$$

which confirms the statement made above about the violation of (2.9).

2.3. *Periodic orbits and pseudo-orbits*

We restrict attention to curves γ that close on themselves after m toroidal transits, during which they make n poloidal transits. The subset of such curves for which S is stationary are, in dynamical systems terminology, periodic orbits with rotation number n/m. In stellarator terminology they are closed field lines with rotational transform $\iota = n/m$, while in tokamak language they are closed field lines with safety factor $q = m/n$.

By the Poincaré–Birkhoff theorem (Arrowsmith & Place 1991: Lichtenberg & Lieberman 1992; Meiss 1992) the periodic orbits occur in pairs, one member of which is a minimax or saddle point of the action and is either stable, or hyperbolic with reflection, while the other corresponds to a minimum of the action and is always unstable (hyperbolic). When the action-saddle-point orbit is stable (elliptic), it forms the centre of an island chain, while the action-minimizing orbit is in the chaotic separatrix region of the island chain. We refer to the intersections of these two classes of orbit with a Poincaré surface of section (e.g. $\zeta = \text{const}$) as O-points and X-points respectively.

By analogy with the construction in Dewar & Khorev (1995) of almost-invariant curves for area-preserving maps, we consider a continuous one-parameter family of periodic curves $\gamma(\theta_0')$ with rotational transform n/m. We can label the curves with any one of θ_i', $0 \leqslant i < m$, the poloidal angles of intersection of γ with the

Poincaré surface of section. We have chosen θ_0'. Since we seek to include the true field lines in this family, we term the other members of the family *pseudo* field lines (pseudo-orbits). Denote θ_i' for a true periodic orbit by θ_i and assume that $\gamma(\theta_0)$ and $\gamma(\theta_j)$ coincide, where θ_j is the physically closest intersection to θ_0. Then the family of pseudo-orbits $\{\gamma(\theta_0') \,|\, \theta_0 \leqslant \theta_0' < \theta_j\}$ makes up a complete toroidal surface Γ.

We end this section by deriving a form of the action gradient involving the magnetic field explicitly. First we find a useful identity relating $\dot{\theta}$ and $\dot{\psi}$ by considering the 'velocity' along γ

$$\dot{\mathbf{r}} \equiv (\dot{\psi}\nabla\theta \times \nabla\zeta + \dot{\theta}\nabla\zeta \times \nabla\psi + \nabla\psi \times \nabla\theta)\mathcal{J} \,, \tag{2.16}$$

where $\mathcal{J} \equiv (\nabla\psi.\nabla\theta \times \nabla\zeta)^{-1}$. We now annihilate the left-hand side by dotting with any vector, $\mathbf{n}$ say, orthogonal to $\dot{\mathbf{r}}$, to find the identity

$$\dot{\theta}\,\mathbf{n}.\nabla\zeta \times \nabla\psi + \mathbf{n}.\nabla\psi \times \nabla\theta = -\dot{\psi}\,\mathbf{n}.\nabla\theta \times \nabla\zeta \,. \tag{2.17}$$

In the context of the construction of the torus Γ from a family of periodic pseudo-orbits, it is natural to take $\mathbf{n}$ to be the unit outward normal to Γ.

Dotting (2.1) with $\mathbf{n}$ and using (2.8) and (2.17), we find

$$B_n = -\left(\dot{\psi} + \frac{\partial\chi}{\partial\theta}\right)\mathbf{n}.\nabla\theta \times \nabla\zeta \,, \tag{2.18}$$

where $B_n \equiv \mathbf{n}.\mathbf{B}$. Comparing this with (2.15), we see that

$$\frac{\delta S}{\delta\theta} = \frac{B_n}{C_n} \,, \tag{2.19}$$

where $C_n \equiv \mathbf{n}.\mathbf{C}$, with $\mathbf{C} \equiv \nabla\theta \times \nabla\zeta$.

3. Ghost surfaces

The curves γ for which the action gradient $\delta S/\delta\theta$ vanishes are invariant under the flow. This suggests that any strategy for defining an almost-invariant curve should minimize the magnitude of the action gradient.

Our first strategy, a direct analogue of the ghost-curve method for area-presersving maps (Angenent & Golé 1991; Golé 1992; MacKay & Muldoon 1993), is to seek the curve corresponding to the O-point closed field line (periodic orbit) with rotational transform n/m, a saddle point of the action, and then to follow the paths of steepest descent on either side of the saddle, down to the neighbouring action-minimizing X-point closed field lines (hyperbolic periodic orbits). This defines a family, γ_τ say, which serves to define a torus in the manner described in § 2.3. The steepest-descent path is defined by the gradient flow

$$\frac{\partial\theta_\tau(\zeta)}{\partial\tau} = -\frac{\delta S}{\delta\theta} \,, \tag{3.1}$$

where $\theta_\tau(\zeta)$ is the trajectory that defines γ_τ through (2.8). By this construction, we automatically capture the invariant sets formed by the two periodic orbits and fill the surface in between in a way that in a sense minimizes the deviation of the pseudo-orbits from invariance.

In the integrable situation, a reinterpretation of ghost surfaces is required. The periodic solution curves are degenerate, and one no longer can distinguish a minimizing or a minimax orbit. Also, the gradient flow becomes zero in the required

direction. One then chooses any one periodic orbit and deforms it, while not increasing the action, to form all the other members of the family making up the ghost surface. The direction of deformation is given by the eigenvector of the Hessian that corresponds to the zero eigenvalue.

3.1. *Ghost pseudo-orbits*

As yet, there remains the problem of how to represent a continuous trajectory in phase space and in particular to evaluate the action along an arbitrary periodic curve. The curve, being periodic, may be expressed as a Fourier series. The action evaluated on this curve over a periodicity length will then be a function of the Fourier components. Alternatively, a discrete set of points describing the curve may be used to fit a spline curve. In this paper, perhaps the least sophisticated method (but also the simplest both intuitively and mathematically) of a piecewise-linear representation is used to approximate the trajectory in phase space. A continuous trajectory is determined by straight line segments through a discrete set of position coordinates y_i labelled as nodes. The action then becomes a function of the y_i, and the problem is reduced to finite dimensions. Only periodic orbits of type (n, m) are considered, and hence a constraint must be enforced :

$$y_{i+mN} = y_i + 2\pi n. \tag{3.2}$$

The dimensionality of the problem becomes mN , where N is the number of segments per 2π in the z direction. Note that as m increases, so does the length of the gradient vector and the Hessian.

The piecewise-linear curve is denoted by $\bar{\gamma}$ and is specified by mN values $y_{i=1,\ldots,mN}$. Note that in each region (z_{i-1}, z_i) the position and velocity are given by

$$y = \frac{y_i(z - z_{i-1}) + y_{i-1}(z_i - z)}{\Delta z}, \tag{3.3}$$

$$\dot{y} = \frac{y_i - y_{i-1}}{\Delta z} \quad \text{for} \quad z \in [z_{i-1}, z_i] \tag{3.4}$$

The velocity is discontinuous, but it is discontinuous on a set of measure zero and the action integral is well defined. Accordingly, a high number of segments in the piecewise-linear approximation are required to accurately describe the trajectories, particularly for higher-order resonances.

The action becomes a function of mN variables, namely the $y_{i=1,\ldots,mN}$, instead of a function of a continuous curve. The action integral is decomposed into a summation of integrals over each segment of the curve. These integrals may now be evaluated, since the functional form for the curve in each region is now known, and the integral becomes a simple integral over the variable z:

$$S[\bar{\gamma}] = S[\{y_i\}] = \sum_{i=1}^{mN} S_i = \sum_{i=1}^{mN} \int_{z_{i-1}}^{z_i} \varphi(\dot{y}, y, z)\, dz, \tag{3.5}$$

where S_i is the action of the straight line segment from z_{i-1} to z_i. This may be evaluated using the Simpson's rule approximation. Expressions for the action gradient and the Hessian may be derived, and are provided in the appendix.

3.2. *Location of extremal curves*

We now have a means of approximating the infinite-dimensional continuous-time phase-space trajectory. An arbitrary curve may be varied until it satisfies the

Euler–Lagrange equations to obtain a real physical trajectory. Alternatively, one may vary the curve until the action becomes a minimum. The minimal curve is actually the unstable trajectory.† This corresponds to the X-point on Poincaré cross-sections. A first guess for the approximating curve can be taken to coincide with this point. Even though the actual trajectory evolves in time in an unstable manner, the method of minimizing a function along a trial curve specified by mN variables is quite simple. No reliance on attempting to follow chaotic field lines is required. A good approximation to the unstable, minimal orbit may be found. The NAG algorithm E04KCF was used to do this.

To locate the saddle curve, it is necessary to locate a zero of the gradient vector. Typically, one would proceed using a multidimensional Newton's method utilizing the Hessian. In such a procedure, a problematical aspect of ghost surfaces is encountered. For close-to-integrable systems, one runs into the difficulty of inverting an ill-conditioned matrix, since the Hessian typically has a very small eigenvalue. This is a direct consequence of the degeneracy of periodic solutions in the integrable limit. The inversion of the Hessian was achieved using singular-value decomposition (Press *et al.* 1983). This technique is designed to invert singular or nearly singular matrices and locates the eigenvectors corresponding to the non-zero eigenvalues. In this application the Hessian has only one small (negative) eigenvalue (MacKay & Muldoon 1993).

To check that the saddle curve has been located succesfully, one may check that the Hessian evaluated at the saddle curve has only one negative eigenvalue and the elements of the corresponding eigenvector are the same sign. Also, one may check that the action evaluated on the minimal curve is lower than the action evaluated along the saddle curve, and that both curves have zero gradient. The single negative eigenvalue indicates that the single direction along which the action integral decreases is the direction specified by its associated eigenvector.

The construction of the gradient flow requires the integration of a system of mN ordinary differential equations. The integration variable was chosen as the y coordinate of the intersection of the ghost surface and the plane $z = 0$.

4. Quadratic-flux minimizing surfaces

4.1. *Definition*

We define the magnetic flux entering or leaving the torus Γ as (Dewar *et al.* 1994)

$$\varphi_1 \equiv \frac{1}{2}\int_\Gamma |B_n|\, d\sigma\,. \tag{4.1}$$

Here $d\sigma = d\theta\, d\zeta / C_n$ is an element of surface area, where $C_n \equiv \mathbf{n}.\nabla\theta \times \nabla\zeta$, with $\mathbf{n}$ the unit normal to Γ at the point defined by (θ, ζ). We see that from (2.19)

$$\varphi_1 = \frac{1}{2}\int\!\!\int_0^{2\pi} d\theta\, d\zeta \left|\frac{\delta S}{\delta\theta}\right|\,. \tag{4.2}$$

As argued in Dewar *et al.* (1994), φ_1 is not an appropriate objective functional for defining almost-invariant surfaces for magnetic field-line flow. Instead, we use (4.2)

† This is consistent with stable motion occurring near potential minima. A minimum of the action corresponds to a motion along which the Lagrangian is minimal. Since $L = T - V$, the greater the potential the lower the Lagrangian. Unstable trajectories occur near maximum potentials.

to motivate the definition of a second moment, or *quadratic-flux* functional

$$\varphi_2 = \frac{1}{2}\iint_0^{2\pi} d\theta\, d\zeta \left(\frac{\delta S}{\delta \theta}\right)^2 . \tag{4.3}$$

Using (2.19), we can express this in terms of the magnetic field as

$$\varphi_2 = \frac{1}{2}\int_\Gamma \frac{B_n^2}{C_n}\, d\sigma. \tag{4.4}$$

With the choice $\mathbf{C} = \nabla\theta \times \nabla\zeta$, (4.4) is identical with that defined by Dewar *et al.* (1994). The mysterious weighting factor $1/C_n$ is now seen to arise naturally from minimization of the action gradient in least squares over the surface. Assuming that the level surfaces of θ and ζ never become tangential to Γ, i.e. that they are suitable coordinates on the torus, the transversality condition $C_n \neq 0$ is satisfied everywhere.

This definition of $\mathbf{C}$ depends on the underlying angle coordinates θ and ζ. If a nearby integrable field is known, with a preferred toroidal angle, then it is natural to choose the action-angle coordinates for this system. The coordinate dependence of (4.3) results from a preferred coordinate representation of $\mathbf{C}$. If $\mathbf{C}$ is given as an arbitrary transverse, divergence-free field then the quadratic-flux integral is independent of the coordinates, as shown by Dewar *et al.* (1994).

The Euler–Lagrange equation resulting from (4.4) is (Dewar *et al.* 1994)

$$\mathbf{B}_\star.\nabla\nu = 0\,, \tag{4.5}$$

where $\mathbf{B}_\star \equiv \mathbf{B} - \nu\mathbf{C}$ and $\nu \equiv B_n/C_n$. We call $\mathbf{B}_\star$ the pseudo-field and ν the non-integrability parameter. From (2.19), ν is seen to be the negative of the action gradient.

Although the magnetic-field form of φ_2, (4.4), does not depend explicitly on the pseudo-orbit concept, we see from (4.5) that pseudo-orbits emerge naturally as the characteristics of the Euler–Lagrange equation. In fact, they are the closed lines of force of the pseudo-field $\mathbf{B}_\star$. Equation (4.5) shows that ν is constant on such a periodic pseudo-orbit. In particular, ν is zero on the true physical periodic orbits, or closed field lines. Thus the invariant dynamics of an island chain can be captured by including its periodic orbits in both the ghost-surface construction and the quadratic-field line minimization method.

4.2. *Quadratic-flux minimizing pseudo-orbits*

To construct a quadratic-flux minimizing surface Γ, we start with a true periodic orbit, which forms the first member of the family of pseudo-orbits making up the surface. The normal component of $\mathbf{B}$ is zero, so $\nu = 0$ on such an orbit. By continuity, for small non-zero ν, $\mathbf{B}_\star$ will have a periodic orbit that is near to the original real periodic orbit. Thus, by varying ν and locating the corresponding periodic pseudo-orbit, a family of periodic pseudo-orbits could be found to form the quadratic-flux minimizing surface.

Specifying ν directly requires a search in the two dimensions (ρ, θ), but this can be difficult in practice because there are typically two periodic pseudo-orbits with the same ν, except where they merge at a tangent bifurcation (Dewar & Khorev 1995). For ν greater than the value at this bifurcation, the search will fail. Thus parametrizing the pseudo-orbits by ν itself is not practical. Also, for configurations close to

nested integrability, the range of ν will be very small, again making ν unsuitable for parametrization purposes.

A more robust method is to specify instead θ and to search in the two dimensions (ρ, ν) for a periodic solution, which will exist uniquely. We have implemented this strategy successfully by adapting Broyden's method (Press *et al.* 1983), which gives convergence to very high precision in a few iterations. The initial guess of $\nu = 0$ (which would be the case for all θ in the integrable limit) and an estimate for the radial location of the perturbed periodic orbits found from the unperturbed location (see § 5, (5.2)) were found to be good choices.

Surfaces for arbitrarily high m could be constructed for about the same computation time by exploiting the periodicity constraints. The entire surface is described by following only those (n, m) periodic pseudo-orbits within a poloidal angular range of about $2\pi/m$, around m toroidal transits.† This construction avoids previous problems encountered when constructing flux surfaces of low rational rotational transform in the integrable limit. The efficiency of field-line tracing methods becomes poor (Reiman & Pomphrey 1991) as the number of toroidal transits required to adequately sample the surface become large. Yet the emergence of the parameter ν seems to allow a freedom that enables one to adequately sample periodic surfaces of high-order rational (rationals with large denominators) rotational transform as simply as those of low-order rational rotational transform.

5. *ABC* magnetic field

Our ultimate interest is the study of stellarator magnetic fields, but the calculation of realistic stellarator fields is time consuming so in this paper we use a simple model field that is, like a general stellarator field, both non-integrable and topologically toroidal. This is achieved by using a magnetic field that is periodic in two directions (y and z) and identifying points one period apart.

We also require the field to have a nowhere-vanishing toroidal component and a monotonic rotational transform, similar to the twist condition often used when analysing area-preserving maps (Dewar & Meiss 1992). This avoids the complications that occur when there is a region of vanishing magnetic shear in the plasma (Hayashi *et al.* 1995; Davidson *et al.* 1995) and the inapplicability of the Poincaré–Birkhoff theorem (Howard & Humphreys 1995).

A simple field that satisfies these criteria is the modified *ABC* field

$$\left.\begin{aligned} B_x(x,y,z) &= A\sin z + C\cos y, \\ B_y(x,y,z) &= B\sin x + A\cos z + \alpha x, \\ B_z(x,y,z) &= C\sin y + B\cos x + B_{z0}\,. \end{aligned}\right\} \tag{5.1}$$

This field differs from the usual *ABC* field in that the extra terms αx and B_{z0} are included to give the field shear in the y direction and a constant component in the z direction. The z coordinate plays the role of the toroidal coordinate, the y coordinate that of the poloidal angle and the x coordinate acts as a radial coordinate. Note that the periodicity length in both the y and z directions is 2π, and with $B_{z0} > B + C$ the 'toroidal' component of the field is nowhere-vanishing. The model retains the simplicity of Cartesian coordinates, with the contravariant

† In the positive θ direction, the next closest intersection point with the Poincaré section will be the point obtained by following the trajectory around l toroidal transits, where $ln \equiv 1 \pmod m$.

and covariant basis vectors being $\mathbf{i}, \mathbf{j}, \mathbf{k}$ and the Jacobian being equal to 1. Unlike toroidal systems, negative values of the radius-like variable (in this case x) are defined.

For the integrable case $A = B = C = 0$, the radial-like coordinate x is a constant of the motion, and the angle y increases linearly in 'time' z at a rate $\alpha x/B_{z0}$. This is in direct analogy with action-angle variables. If we denote by (x_j, y_j) the intersection points of a continuous trajectory with the toroidal surface of section $z = 0$ then we obtain a discrete trajectory that characterizes the continuous trajectory. This method is the Poincaré mapping formalism of Hamiltonian mechanics (Lichtenberg & Lieberman 1992; Arrowsmith & Place 1991). Periodic orbits are those that satisfy $y_{j+mN} = y_j + 2\pi n$ and are found at radial locations given by

$$\frac{B_y}{B_z} = \frac{n}{m} = \frac{\alpha x}{B_{z0}} \,. \tag{5.2}$$

With A, B and C all non-zero, chaotic trajectories are created.

We construct the field-line Hamiltonian and canonical momentum by integrating (2.2)–(2.4)

$$\bar{\chi}(x, y, z) = \tfrac{1}{2}\alpha x^2 - B\cos x + Ax\cos z + f(y, z), \tag{5.3}$$

$$\bar{\psi}(x, y, z) = B_{z0}x + B\sin x + Cx\sin y + g(y, z). \tag{5.4}$$

Here f and g are arbitrary other than being required to satisfy

$$\partial_z\bar{\psi} + \partial_y\bar{\chi} = -B_x \,, \tag{5.5}$$

which is solved by

$$f(y, z) = C\sin y \,, \quad g(y, z) = B\sin x \,. \tag{5.6}$$

The velocity $\dot{y}$ is constructed from Hamilton's equations in the canonical coordinates (ψ, y, z) as

$$\dot{y}(x, y, z) = \partial_\psi\chi(\psi, y, z) = \frac{\partial_x\bar{\chi}(x, y, z)}{\partial_x\bar{\psi}(x, y, z)} = \frac{\alpha x + B\sin x + A\cos z}{B_{z0} + B\cos x + C\sin y} \,. \tag{5.7}$$

This is solved numerically for $x = \tilde{x}(\dot{y}, y, z)$ to obtain the Lagrangian

$$\varphi(\dot{y}, y, z) = \psi(\tilde{x}(\dot{y}, y, z), y, z)\dot{y} - \bar{\chi}(\tilde{x}(\dot{y}, y, z), y, z) \,. \tag{5.8}$$

6. Quadratic-flux minimizing surfaces for the ABC field

Several quadratic-flux minimizing surfaces have been calculated for various perturbations of the ABC field and are shown in the following figures. Three surfaces are shown in figure 1. For low perturbations, periodic pseudo orbits of arbitrarily high order were easily located. Cross-sections of many surfaces are shown in figure 2. As the perturbation increases, chaotic regions grow, and the method used to locate the periodic pseudo orbits becomes more unstable and problems are encountered for the higher periodicities. Nevertheless, quadratic-flux minimizing surfaces are fairly robust, as figure 3 shows. Further evidence indicating the construction of these surfaces is possible in regions of connected chaos is presented in Dewar & Khorev (1995).

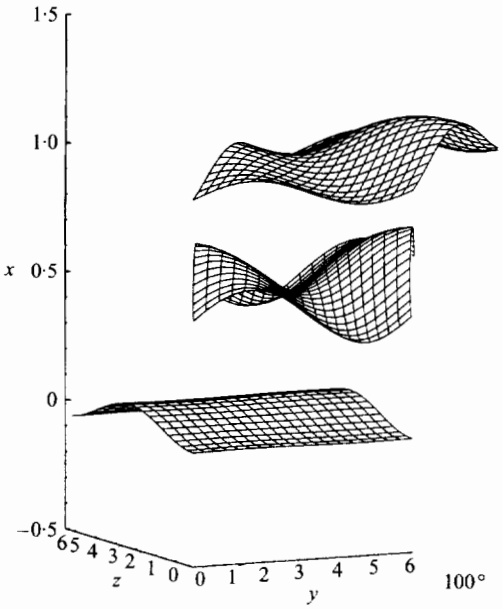

FIGURE 1. Weighted quadratic-flux minimizing surfaces with periodicities $(n, m) = (0, 1), (1, 2)$ and $(1, 1)$ for $A = 0{\cdot}06$, $B = 0{\cdot}06$, $C = 0{\cdot}06$, $B_{zo} = 1$ and $\alpha = 1$.

Numerical evidence cannot prove that surfaces with different periodicities do not intersect, but it may strongly support such claims. Surfaces for nearby rationals were constructed numerically, and are seen to be smooth and non-intersecting for quite large perturbations. They are shown in figure 4. Note also that in figure 4 the $(2, 3)$ surface threads the O- and X-points. This feature is guaranteed because the same integrator was used to construct the Poincaré plot as was used to locate the periodic pseudo-orbits, in particular the real periodic orbits, which correspond exactly to the O- and X-points.

We may note the sinusoidal behaviour of the non-integrability parameter ν, shown in figure 5. The smooth behaviour of this function, the discussion presented regarding the construction of periodic pseudo-orbits and the numerical evidence suggest strongly that quadratic-flux minimizing surfaces are smooth and non-intersecting, at least until chaos has swamped the region and the periodic pseudo-orbits become more difficult to locate.

An island chain of finite width prohibits other island chains (of the same, required, topology) within the resonance. This is seen in figure 2, where the large $(0, 1)$ island has pushed apart the quadratic-flux minimizing surfaces. With the intended construction of a coordinate system, where the surfaces are required to form a continuous radial coordinate, an interpolation is required. A method used presently in PIES (Reiman & Pomphrey 1991: Greenside *et al.* 1989) is that of Fourier decomposing a discrete set of surfaces, then using cubic splines to interpolate the individual Fourier components. This procedure has successfully been applied to quadratic-flux minimizing surfaces constructed for the H-1 Heliac and generalized magnetic flux coordinates have been introduced. This is the topic of ongoing research.

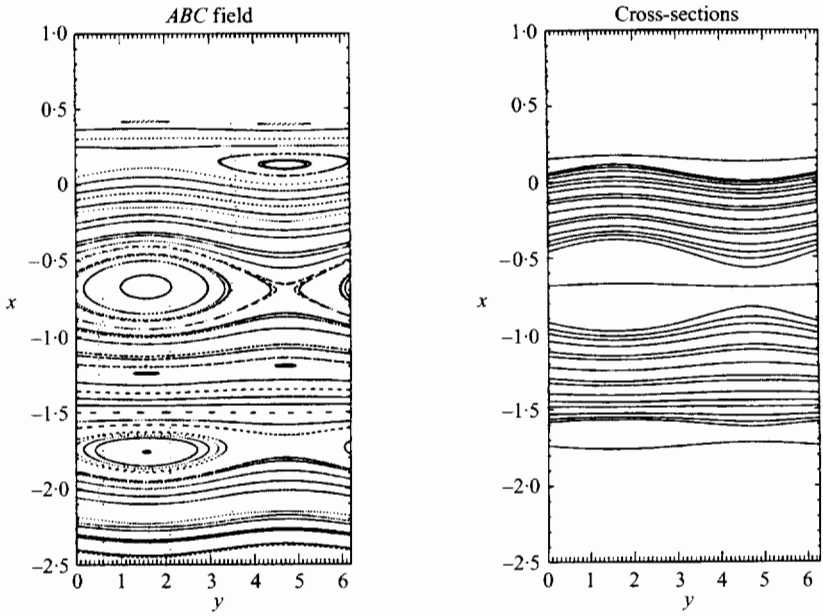

FIGURE 2. Cross-sections of quadratic-flux minimizing surfaces $(n, m) = (0, 1)$, $(\pm 1, 1)$, $(\pm 1, 2)$, $(\pm 1, 3)$, $(\pm 2, 3)$, $(\pm 1, 4)$, $(\pm 3, 4)$, $(\pm 1, 5)$, $(\pm 2, 5)$, $(\pm 3, 5)$, $(\pm 4, 5)$, $(\pm 5, 6)$, $(\pm 2, 7)$, $(\pm 3, 7)$, $(\pm 4, 7)$, $(\pm 5, 7)$ and $(\pm 6, 7)$ compared with a Poincaré cross section of the ABC flow for low perturbation, $A = 1$, $B = 0{\cdot}5$ and $C = 0{\cdot}025$.

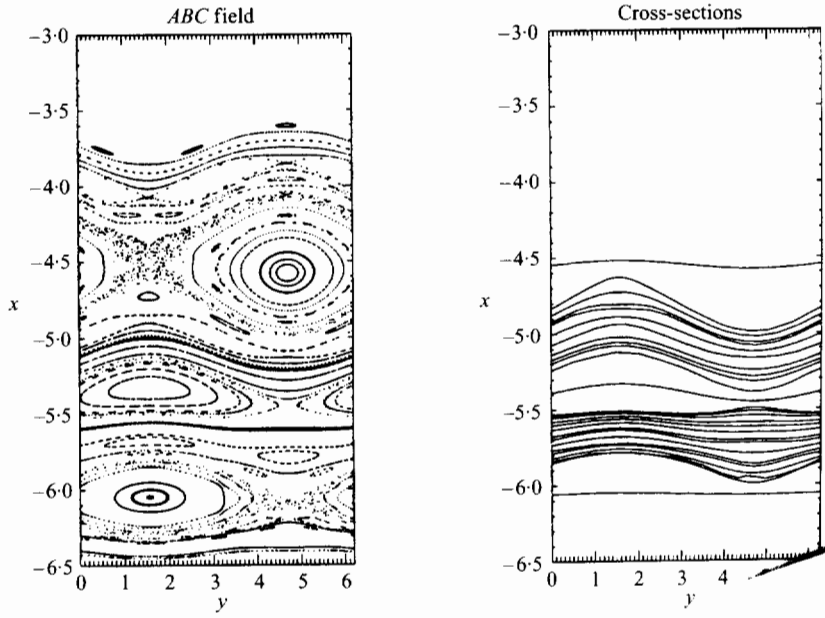

FIGURE 3. Cross-sections of quadratic-flux minimizing surfaces (n, m) $(\pm 1, 2)$, $(\pm 1, 3)$, $(\pm 2, 3)$, $(\pm 1, 4)$, $(\pm 3, 4)$, $(-1, 5)$, $(-2, 5)$, $(\pm 3, 5)$, $(\pm 1, 6)$, $(\pm 3, 7)$, $(\pm 4, 7)$ and $(-5, 7)$ compared with a Poincaré cross section of the AL perturbation, $A = 5$, $B = 0{\cdot}5$ and $C = 0{\cdot}015$.

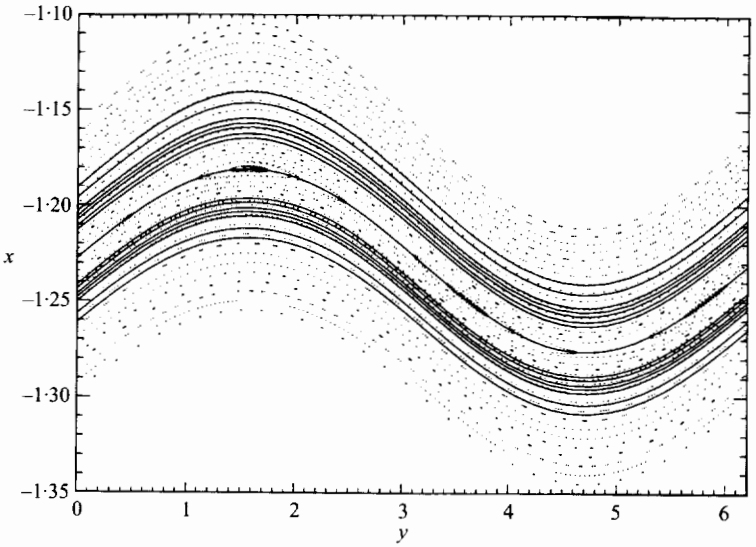

FIGURE 4. Cross-sections of quadratic–flux minimizing surfaces with periodicities $(n, m) = (2, 3)$, $(7, 10)$, $(7, 11)$, $(9, 13)$, $(9, 14)$, $(11, 16)$, $(11, 17)$, $(12, 17)$, $(12, 19)$, $(13, 19)$, $(13, 20)$, $(15, 22)$, $(15, 23)$, $(20, 29)$ and $(20, 31)$; $A = 2$, $B = 0{\cdot}1$ and $C = 0{\cdot}01$.

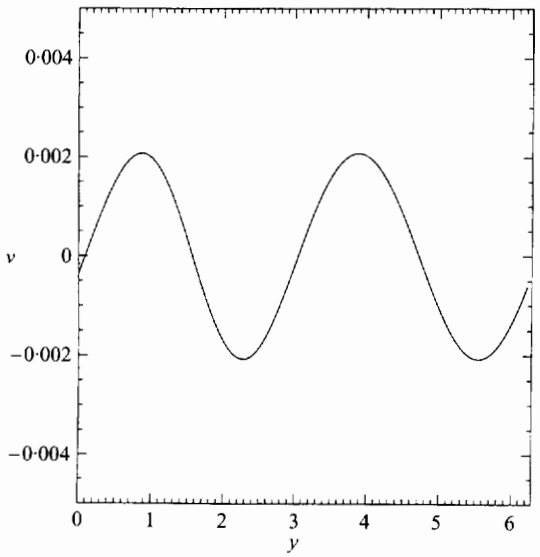

FIGURE 5. Non-integrability parameter ν for $A = 5$, $B = 0{\cdot}5$, $C = 0{\cdot}015$, $p = 1$ and $q = 2$.

7. Ghost surfaces for the ABC field

Several ghost surfaces and their intersection with the Poincaré section are shown in figures 6 and 7 respectively.

It is obvious that, as the number of linear segments used to approximate the continuous curve is increased, the accuracy will improve. A more precise test of this is achieved as follows. A very good approximation to the stable $(1, 1)$ trajectory $y = y(z)$ for $z \in [0, 2\pi]$ can be made by integrating along the magnetic vector field. The stable trajectory is quite easy to locate using Broyden's method. Only the real,

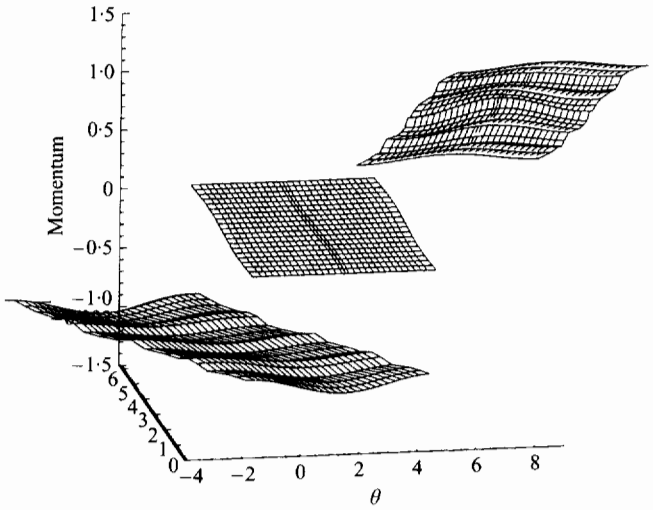

FIGURE 6. Ghost surfaces $(n, m) = (1, 1)$, $(0, 1)$ and $(-1, 1)$.

stable periodic orbit is required, so the search is simply in (ρ, θ) space and there is no non-integrability parameter ν to consider. The approximating piecewise-linear curve $y_{i=1,\ldots,mN}$ can be compared with the actual orbit using a sum of deviations method. One can define a measure of the difference Δ as follows :

$$\Delta = \left\{ \frac{1}{mN} \sum_{i=1}^{mN} [y_i - y(i\Delta z)]^2 \right\}^{\frac{1}{2}}. \tag{7.1}$$

The approximation $y_{i=1,\ldots,mN}$ to the saddle curve was found using about seven iterations of Newton's method, with a singular-value decomposition of the Hessian matrix. The numerical routines SVDCMP and SVBKSB from Press *et al.* (1983) were used. Typically, the zero of the gradient was found to about 10^{-9}. The magnetic field parameters used were $A = 5, B = 0{\cdot}5, C = 0{\cdot}015, B_{z0} = 1$ and $\alpha = 1$. Figure 8 shows the behaviour of this parameter with N. The computation time required for such values increased so much that it became impractical to construct ghost surfaces with high m values, and $N = 20$ was used. Such a value gave reasonable agreement with the smooth position coordinate.

A set of three coordinates was constructed from the curve by associating the constant velocity (which may be converted to a canonical momentum coordinate) with the midpoint of the time and position in each region. Note that the piecewise-linear description of the trajectory implies a discontinuous velocity coordinate. Thus the piecewise-linear approach may be too simple, since it produces a resolution problem. To overcome the poor resolution, the momentum coordinate was smoothed using a three point average. This reduced the irregularities inherent in the piecewise-linear approach.†

The integration of the defining differential equation of ghost surfaces is slow

† Note that averaging the velocity curve has very minor effects on its consistency with the position curve. Since the average of the velocity over a small region is unchanged, the average position curve is unchanged. First-order changes made to the velocity curve become second-order changes to the position curve. This step is consistent with using a piecewise-linear continuous-curve approximation.

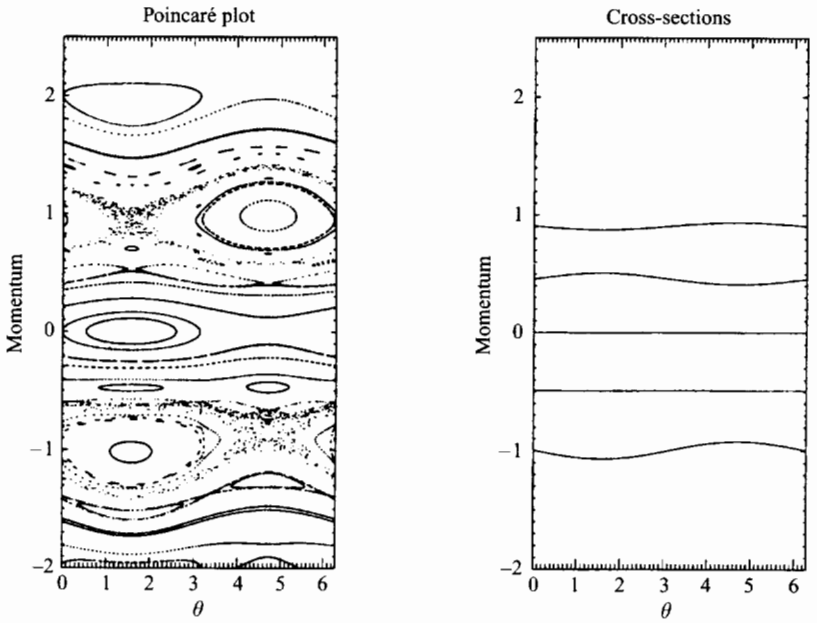

FIGURE 7. Cross-sections of ghost surfaces $(n, m) = (1, 1)$, $(1, 2)$, $(0, 1)$, $(-1, 2)$ and $(-1, 1)$, for $A = 5$, $B = 0{\cdot}5$ and $C = 0{\cdot}015$.

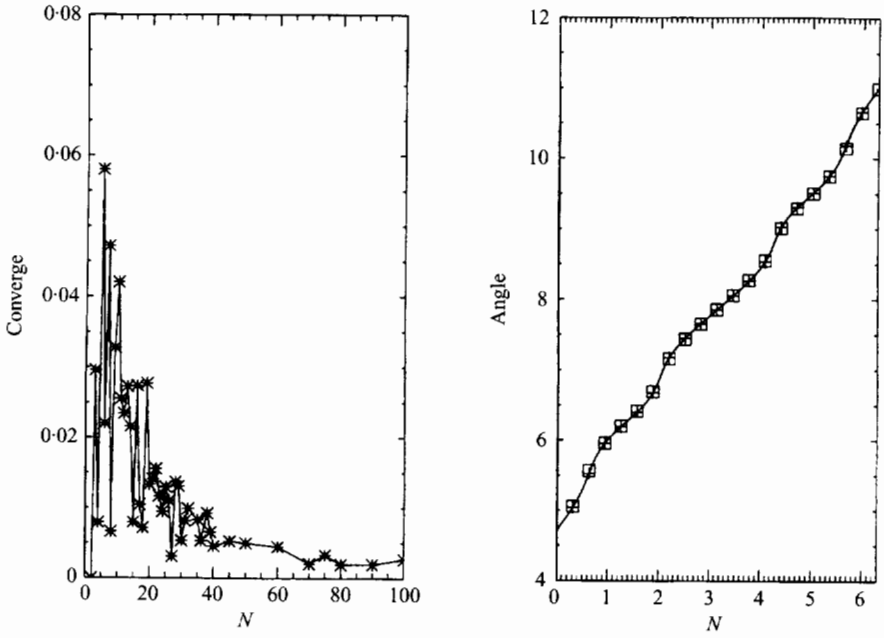

FIGURE 8. Convergence of angle with N: (*a*) angle convergence test: (*b*) angle versus time for a real periodic curve.

A	B	C	B_{z0}	α	λ_1
5	0·5	0·01	1	1	−0·00045
5	0·5	0·02	1	1	−0·00109
5	0·5	0·04	1	1	−0·00288
5	0·5	0·05	1	1	−0·00402
5	0·5	0·07	1	1	−0·00674
5	0·5	0·09	1	1	−0·00997
5	0·5	0·10	1	1	−0·01173
5	0·5	0·20	1	1	−0·02355

TABLE 1. Hessian eigenvalues.

when the system in nearly integrable, but maybe it could be improved by a preconditioned descent algorithm or the adding of an inertia term to the equation (Hirshman & Betancourt 1991). Also, for strong perturbations, bifurcations in phase space may produce two solution curves, of double the periodicity, very close to the original saddle curve and this seems to disrupt the location of the saddle curve.

Table 1 shows the behaviour of the negative eigenvalue of the Hessian calculated for the (1, 1) periodic orbit for various perturbations. As the perturbation is increased, the magnitude of the eigenvalue increases. This is related to the increasing non-degeneracy of the minimal and minimax orbits as one moves away from integrability. The gradient between the orbits also becomes greater.

8. Comparison of ghost surface and quadratic-flux minimizing surface

For $(n, m) = (1, 1)$, and for high accuracy ($N = 50$) in the piecewise-linear approach affordable for such low m, we may compare the curves. The solid line in figure 9 is the cross section of the $(n, m) = (1, 1)$ ghost surface, with the dashed line being the quadratic-flux minimizing surface. The x coordinates of the quadratic-flux minimizing surfaces were converted to the canonical momentum coordinates of the ghost surface construction to enable this comparison.

9. Conclusions

Both the construction of ghost surfaces and quadratic flux-minimizing surfaces have been implemented successfully for a model toroidal field. It has been shown that the construction of quadratic-flux minimizing surfaces is much simpler and quicker, and becomes trivial in the integrable limit. For the study of nearly integrable systems this nice behaviour near integrability is an attractive feature of the quadratic-flux minimizing surface method.

By contrast, the construction of ghost surfaces from a gradient flow curve breaks down at integrability, though this may be overcome by moving along the nullvector of the Hessian matrix of the action functional. What does not appear to be avoidable is the inherent slowness of the ghost-surface method for situations near integrability. Added to this is the complexity of constructing approximating periodic

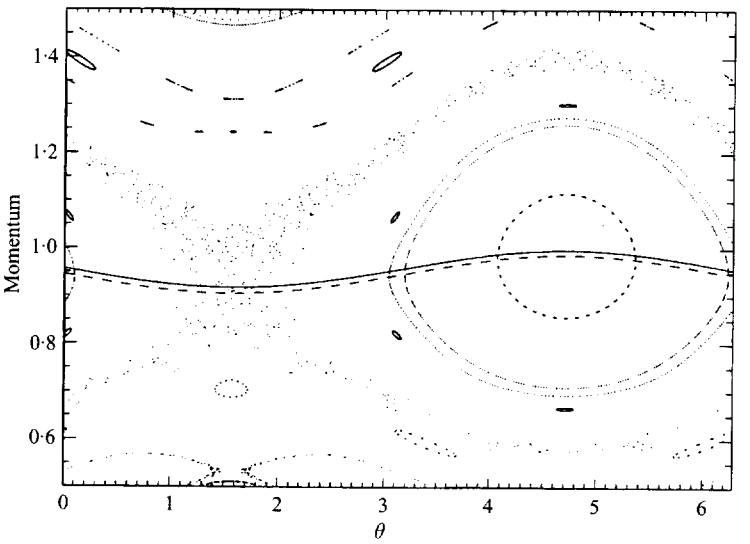

FIGURE 9. Cross-sections of ghost surface and quadratic-flux minimizing surface, (1, 1) for $A = 5$, $B = 0{\cdot}5$ and $C = 0{\cdot}015$.

orbits by some kind of functional representation and the subsequent calculation of the gradient and the typically ill-conditioned Hessian matrix. The construction of the Lagrangian itself requires, in typical magnetic field cases as considered in this paper, a numerical integration to obtain the Hamiltonian and canonical momentum and then a numerical inversion to obtain the velocity function. This latter point only applies when one is transforming from a magnetic field-line description to the Lagrangian/Hamiltonian description, and would not apply if one were given the Lagrangian directly.

One technique employed in PIES to examine non-integrable magnetic fields is the use of 'near-magnetic coordinates' (Greenside *et al.* 1989). This method uses flux surfaces where they exist (though resonant perturbations may have destroyed some flux surfaces, other 'more irrational' surfaces will remain), and interpolates between these surfaces through the chaotic regions. This procedure thus tends to utilize irrational surfaces only, in that perturbations destroy surfaces with rational rotational transform. The KAM theory guarantees the existence of at least some flux surfaces, but for the more irrational frequencies. As a result, one may expect (Greene 1979) that these surfaces are the most deformed surfaces that one may choose. The deformations are caused by resonant perturbations, usually the lower-order rationals, which destroy the rational flux surfaces and deform the irrational surfaces nearby. The most irrational numbers are found near the lowest order rationals, where the resonant pertubation has its greatest influence. The greater the deformation of the surface, the greater the Fourier coefficients required to describe it and the problem of exploding Fourier coefficients is encountered.

For the construction of quadratic-flux minimizing surfaces, however, one chooses low order rationals. Even though these are the flux surfaces that are first destroyed, quadratic-flux minimizing surface are likely to be only slightly deformed. The quadratic-flux minimizing surfaces pass directly through the island chain. The (n, m) Fourier coefficient of the (n, m) surface is likely to be small.

We have shown that the theory of Dewar *et al.* (1994), derived geometrically for

general divergence-free fields, follows naturally from the Lagrangian/Hamiltonian approach. Its beauty is that it is expressed directly in terms of the magnetic field, and thus does not require explicit construction of canonical magnetic-field coordinates and a Hamiltonian. As a result, our numerical method for constructing quadratic-flux minimizing surfaces relies simply on well-established methods for tracing magnetic fields and finding the location of periodic orbits. Since we have shown that the action gradient can be expressed directly in terms of the magnetic field, it may also be possible to formulate a ghost-surfaces theory that does not require explicit construction of the Lagrangian, but it would almost certainly still be more time-consuming, especially near integrability.

The use of pseudo-orbit formalisms allows the problem of constructing approximate action-angle representations to be decomposed conceptually into two distinct phases–the construction of almost-invariant surfaces and the construction of a global coordinate system. In this paper we have addressed only the first problem. There are several issues to be considered before the global problem is fully solved.

One issue is the choice of the poloidal and toroidal angle coordinates $\theta(\mathbf{r})$ and $\zeta(\mathbf{r})$. We have taken these as given, but it is common practice in magnetic confinement physics to regard both the poloidal and toroidal angles as general curvilinear coordinates, to be chosen to simplify the representation of the physics. For instance, in the integrable case straight-field-line coordinates, particularly Boozer coordinates (Boozer 1983), are often preferred.

Another issue is the choice of almost-invariant surface. We have argued that the quadratic-flux minimization principle applied to selected rational rotational transform surfaces provides a robust and practical way of choosing surfaces, but one still needs to select which rationals to work with and to interpolate between them in some suitable smooth fashion. A further point is that the surface problem and the angle problem are not completely decoupled, since in both the ghost-surface and quadratic-flux formulations the action gradient depends on the choice of angle coordinates. Thus the almost-invariant surface will change if the choice of angles is changed.

Meiss & Hazeltine (1990) have pointed out that careful choice of coordinates can make the Hamiltonian representation of guiding-centre motion canonical, even in the non-integrable case. An optimal choice for the global coordinates might thus be one that is canonical in the sense of Meiss and Hazeltine and that reduces to Boozer coordinates in integrable cases.

One of us (S.R.H.) was supported by an Australian National University postgraduate scholarship.

Appendix A. Numerical determination of ghost surfaces

The gradient of the action function is constructed. Note that each S_i is a function of the independent variables y_{i-1} and y_i, that is

$$S_i = S_i(y_{i-1}, y_i). \tag{A 1}$$

The variation in the action of the entire curve is then

$$\delta S[\bar{\gamma}] = \sum_{i=1}^{mN} (\partial_2 S_i + \partial_1 S_{i+1})\, \delta y_i. \tag{A 2}$$

Here ∂_i indicates differentiation with respect to the ith variable of S_i. From this the gradient may be identified:

$$\partial_i S = (\partial_2 S_i + \partial_1 S_{i+1}) = \partial_i S(y_{i-1}, y_i, y_{i+1}). \tag{A 3}$$

Here $\partial_2 S_i$ and $\partial_1 S_i$ are given as

$$\partial_1 S_i = \int_{z_{i-1}}^{z_i} \left[\partial_y \varphi \left(\frac{z_i - z}{\Delta z} \right) - \partial_{\dot{y}} \varphi \left(\frac{1}{\Delta z} \right) \right] dz, \tag{A 4}$$

$$\partial_2 S_i = \int_{z_{i-1}}^{z_i} \left[\partial_y \varphi \left(\frac{z - z_{i-1}}{\Delta z} \right) + \partial_{\dot{y}} \varphi \left(\frac{1}{\Delta z} \right) \right] dz. \tag{A 5}$$

The gradient of a function of mN variables is a vector of length mN. The gradient of the gradient is interpreted as a matrix, called the Hessian or the matrix of second partial derivatives. The Hessian is required since it gives information about the structure of the phase-space trajectories around a certain point when the gradient itself is degenerate. That is, when the gradient is zero along a trajectory, which is the condition for the trajectory to be a physical trajectory, the trajectory itself may be the saddle orbit or the minimal orbit. The Hessian contains information that determines which type of trajectory has been located and also some information on the value of the action evaluated on nearby curves. The Hessian enables the zeros of the gradient to be found efficiently by using an mN dimensional Newton's method. Also, it indicates the single direction (up to scalar multiple) to move away from the saddle orbit so as to decrease the action.

Note that for the piecewise-linear method, each term in the gradient vector ∇S depends on only three of the discrete set of positions y_n, so most of the elements of the Hessian $\nabla^2 S$ will be zero. In fact, the Hessian is a periodic tridiagonal matrix. Its elements are given by

$$\nabla^2 S_{n-1,n} = \partial_{n-1} \partial_n S = \partial_1 \partial_2 S_n, \tag{A 6}$$

$$\nabla^2 S_{n,n} = \partial_n \partial_n S = \partial_2 \partial_2 S_n + \partial_1 \partial_1 S_{n+1}, \tag{A 7}$$

$$\nabla^2 S_{n+1,n} = \partial_{n+1} \partial_n S = \partial_2 \partial_1 S_{n+1}, \tag{A 8}$$

$$\begin{aligned} \partial_1 \partial_1 S_n = & \int_{z_{n-1}}^{z_n} \left(\partial_y \partial_y \varphi \frac{z_n - z}{\Delta z} - \partial_{\dot{y}} \partial_y \varphi \frac{1}{\Delta z} \right) \frac{z_n - z}{\Delta z} \, d\zeta \\ & - \int_{z_{n-1}}^{z_n} \left(\partial_y \partial_{\dot{y}} \varphi \frac{z_n - z}{\Delta z} - \partial_{\dot{y}} \partial_{\dot{y}} \varphi \frac{1}{\Delta z} \right) \frac{1}{\Delta z} \, d\zeta, \end{aligned} \tag{A 9}$$

$$\begin{aligned} \partial_2 \partial_1 S_n = & \int_{z_{n-1}}^{z_n} \left(\partial_y \partial_y \varphi \frac{z - z_{n-1}}{\Delta z} + \partial_{\dot{y}} \partial_y \varphi \frac{1}{\Delta z} \right) \frac{z_n - z}{\Delta z} \, d\zeta \\ & - \int_{z_{n-1}}^{z_n} \left(\partial_y \partial_{\dot{y}} \varphi \frac{z - z_{n-1}}{\Delta z} + \partial_y \partial_{\dot{y}} \varphi \frac{1}{\Delta z} \right) \frac{1}{\Delta z} \, d\zeta, \end{aligned} \tag{A 10}$$

$$\begin{aligned} \partial_2 \partial_2 S_n = & \int_{z_{n-1}}^{z_n} \left(\partial_y \partial_y \varphi \frac{z - z_{n-1}}{\Delta z} + \partial_y \partial_y \varphi \frac{1}{\Delta z} \right) \frac{z - z_{n-1}}{\Delta z} \, d\zeta \\ & + \int_{z_{n-1}}^{z_n} \left(\partial_y \partial_y \varphi \frac{z - z_{n-1}}{\Delta z} + \partial_y \partial_{\dot{y}} \varphi \frac{1}{\Delta z} \right) \frac{1}{\Delta z} \, d\zeta. \end{aligned} \tag{A 11}$$

The structure of the Hessian is as follows:

$$\begin{pmatrix} \nabla^2 S_{1,1} & \nabla^2 S_{1,2} & \cdots & & & & \cdots & \nabla^2 S_{1,mN} \\ \nabla^2 S_{2,1} & \nabla^2 S_{2,2} & \nabla^2 S_{2,3} & \cdots & & & & \\ \vdots & \nabla^2 S_{3,2} & \nabla^2 S_{3,3} & \nabla^2 S_{3,4} & \cdots & & & \\ & \vdots & \nabla^2 S_{4,3} & \nabla^2 S_{4,4} & \nabla^2 S_{4,5} & \cdots & & \vdots \\ & & \vdots & \vdots & \vdots & & & \\ & & & & & & & \\ \nabla^2 S_{mN,1} & \cdots & & & & \cdots & \nabla^2 S_{mN,mN-1} & \nabla^2 S_{mN,mN} \end{pmatrix}.$$

If cubic splines were used instead of the piecewise-linear description, the Hessian would be a periodic quin-diagonal. In the Fourier approach, generally none of the terms would be zero. The description of a continuous curve using finitely many parameters reduces the infinite dimensionality of the Hessian to something more manageable.

REFERENCES

Angenent, S. & Golé, C. 1991 Lamination by ghost circles. Technical Report, Forschungsinstitut für Mathematik, ETH, Zürich.

Arrowsmith, D.K. & Place, C.M. 1991 *An Introduction to Dynamical Systems*. Cambridge University Press.

Boozer, A.H. 1982 Establishment of magnetic coordinates for given magnetic field. *Phys. Fluids* **25**, 520.

Boozer, A.H. 1983 Evaluation of the structure of ergodic fields. *Phys. Fluids* **26**, 1288.

Cary, J.R. & Hanson, J.D. 1986 Stochasticity reduction. *Phys. Fluids* **29**, 2464.

Cary, J.R. & Littlejohn, R.G. 1983 Noncanonical Hamiltonian mechanics and its application to magnetic field line flow. *Ann. Phys. (NY)* **151**, 1.

Davidson, M., Dewar, R.L., Gardner, H.J. & Howard, J. 1995 Hamiltonian maps for Heliac magnetic islands. *Aust. J. Phys.* **48**, 871.

Dewar, R.L. & Khorev, A.B. 1995 Rational quadratic-flux minimizing circles for area-preserving twist maps. *Physica* **D85**, 66.

Dewar, R.L. & Meiss, J.D. 1992 Flux-minimizing curves for reversible area-preserving maps. *Physica* **D57**, 476.

Dewar, R.L., Hudson, S.R. & Price, P. 1994 Almost invariant manifolds for divergence free fields. *Phys. Lett.* **194A**, 49.

D'haeseleer, W.D., Hitchon, W.N.G., Callen, J.D. & Shohet, J.L. 1983 *Flux Coordinates and Magnetic Field Structure*. Springer-Verlag, Berlin.

Goldstein, H. 1980 *Classical Mechanics*, 2nd edn. Addison-Wesley, Reading, MA.

Golé, C. 1992 Partition by ghost circles. *J. Differential Eqns* **97**, 140.

Greene, J.M. 1979 A method for determining a stochastic transition. *J. Math. Phys.* **20**, 1183.

Greenside, H.S., Reiman, A.H., & Salas, A. 1989 Convergence properties of a nonvariational 3D MHD code. *J. Comput. Phys.* **81**, 102.

Hanson, J.D. 1994 Correcting small magnetic field non-axisymmetries. *Nucl. Fusion* **34**, 441.

Hanson, J.D. & Cary, J.R. 1984 Elimination of stochasticity in stellarators. *Phys. Fluids* **27**, 767.

HAYASHI, T., SATO, T., GARDNER, H.J. & MEISS, J.D. 1995 Evolution of magnetic islands in a Heliac. *Phys. Plasmas* **2**, 752.

HIRSHMAN, S.P. & BETANCOURT, O. 1991 Preconditioned descent algorithm for rapid calculations of magnetohydrodynamic equilibria. *J. Comput. Phys.* **96**, 99.

HOWARD, J.E. & HUMPHREYS, J. 1995 Nonmonotonic twist maps. *Physica* **D80**, 256.

KAASALAINEN, M. & BINNEY, J. 1994 Construction of invariant tori and integrable Hamiltonians. *Phys. Rev. Lett.* **73**, 2377.

LICHTENBERG, A.J. & LIEBERMAN, M.A. 1992 *Regular and Chaotic Dynamics,* 2nd edn. Springer-Verlag, New York.

MACKAY, R.S. & MULDOON, M.R. 1993 Diffusing through spectres: ridge curves, ghost circles and a partition of phase space. *Phys. Lett.* **178A**, 245.

MEISS, J.D. 1992 Symplectic maps, variational principles and transport. *Rev. Mod. Phys.* **64**, 362.

MEISS, J.D. & HAZELTINE, R.D. 1990 Canonical coordinates for guiding center particles. *Phys. Fluids* **B2**, 2563.

PRESS, W. H., FLANNERY, B. P., TEUKOLSKY, S. A., & VETTERLING, W. T. 1983 *Numerical Recipes in Fortran.* Cambridge University Press.

REIMAN, A. & POMPHREY, N. 1991 Computation of magnetic coordinates and action angle coordinates. *J. Comput. Phys.* **94**, 225.

YOSHIDA, Z. 1994 A remark on the Hamiltonian form of the magnetic-field-line equations. *Phys. Plasmas* **1**, 208.